



Optimizing the optical and magneto-optical response of all-dielectric metasurfaces with tilted side walls

SIYUAN GAO,^{1,*} YASUTOMO OTA,^{2,4}  FENG TIAN,¹ TIANJI LIU,³
AND SATOSHI IWAMOTO¹ 

¹Research Center for Advanced Science and Technology, The University of Tokyo, Meguro, Tokyo 153-8904, Japan

²Department of Applied Physics and Physico-Informatics, Keio University, Yokohama, Kanagawa 223-8522, Japan

³GPL Photonics Laboratory, State Key Laboratory of Luminescence and Applications, Changchun Institute of Optics, Fine Mechanics and Physics, Chinese Academy of Sciences, Changchun, Jilin 130033, China

⁴ota@appi.keio.ac.jp

*gaosy@iis.u-tokyo.ac.jp

Abstract: All-dielectric metasurfaces based on ferrimagnetic iron garnets are a promising platform for realizing ultra-compact magneto-optical (MO) devices with low loss. However, ferrimagnetic iron garnets are notorious for being intractable on fine nanopatterning, hindering the faithful fabrication of designed nanostructures. In this regard, it is important to assess the influence of fabrication imperfections on the performance of MO metasurfaces. Here, we investigate the optical properties of a MO metasurface with structural imperfections. As the most typical fabrication error, we studied the impact of the tilted side walls of cylindrical garnet disks that constitute the metasurfaces. We found that tilting the side walls drastically degrades the MO response and light transmittance of the device. Nevertheless, it was also found that the performance can be recovered by optimizing the refractive index of the material covering the upper half of the nanodisks.

© 2023 Optica Publishing Group under the terms of the [Optica Open Access Publishing Agreement](#)

1. Introduction

Magneto-optical (MO) materials are commonly used for realizing non-reciprocal optical devices including isolators and circulators. Among all MO media in the optical domain, ferrimagnetic iron garnets, such as yttrium iron garnet ($\text{Y}_3\text{Fe}_5\text{O}_{12}$, YIG), have been the first choice of material because they exclusively exhibit both moderate MO responses and high optical transparency [1] at room temperature. However, the relatively weak MO effect tends to make the MO devices bulky. Indeed, most commercially available MO devices are millimeter-scale or larger, limiting their potential for finding further applications.

An important approach to boost MO effect is to employ optical resonances. An earlier attempt employed a distributed Bragg reflector to confine light within an intentionally introduced defect region, which resulted in the improved Faraday rotation angle (θ_f) at the resonance [2,3]. However, the overall device became thick due to the presence of the Bragg reflector [4–6]. Moreover, the experimentally obtained light transmittance (T) was rather low and thus the resulting value of the figure of merit ($FoM = \sqrt{T} \cdot |\theta_f|$) was significantly degraded. Plasmonic resonators are another route to enhance MO response and enable the extreme confinement of light to the nanoscale [7–12]. However, ohmic losses in metals intrinsically hamper high light transmittance and Faraday rotation angle of such devices and thus high FoM as well [9,13–16].

Recently, an all-dielectric MO metasurface has been numerically demonstrated to attain both a large θ_f of 7.5° and a high T of 96% with 260 nm-thick nanostructure [17]. The structure consists of a square lattice of nanodisks made of Bismuth Iron Garnet (BIG), which support

electric dipole (ED) and magnetic dipole (MD) modes [18]. The tight light confinement in the two optical modes increased θ_f , while the high T was obtained with electromagnetically induced transparency (EIT) by spectrally and spatially overlapping the two modes [19–21]. Further improvement of the device performance was numerically demonstrated by structural optimization with a Bayesian optimization algorithm [22].

While numerical studies on all-dielectric MO metasurfaces made progress [23], it is rather challenging to experimentally perform nanopatterning of garnet materials, which are physically very hard and inert to dominant chemistry. Brute-force approaches are often employed for nanostructuring of garnets, such as focused ion beam (FIB) milling [24,25]. However, with such an approach, it is extremely difficult to achieve faithful patterning in the nanoscale. Patterned deposition of garnets is a promising alternative [26,27]. However, high quality garnets are obtained only when using limited combinations of garnets and substrates, such as YIG on gadolinium iron garnet (GGG). Unfortunately, YIG and GGG are very close in their refractive indices and thus not suitable for tight light confinement. Conventional nanofabrication using dry etching has also been examined for realizing garnet-based nanophotonic structures [24,28–30]. However, it is extremely difficult to make the etched sidewalls vertical. Therefore, most experimentally realized structures accompanied with tilted side walls, which are neglected in most of theoretical studies. Note that, very recently, there was an experimental demonstration of a MO metasurface based on a Si resonator placed on a YIG film [31,32]. This method facilitates faithful fabrication by avoiding patterning of YIG itself but has not yet achieved a sufficiently high θ_f and T .

Here, we study MO metasurfaces based on periodic arrays of garnet truncated cones with tilted side walls. We investigated the impact of non-vertical sidewall angles (α_c) on θ_f and T of the truncated cones. We found that both θ_f and T were rapidly degraded by deviating α_c from 90° . Whereas it was also found that the degradation can be mitigated by optimizing the refractive index of embedding material above the nanodisks. We believe that this study is an important step toward the experimental realization of ultra-thin MO Faraday rotators, isolators, and magnetic field sensors.

2. Device structure and numerical simulation methods

We investigated a MO all-dielectric metasurface composed of an infinite periodic square array of BIG nanodisks embedded in SiO_2 (Fig. 1). BIG is responsible for MO effects in this system and is described by a relative permeability $\mu_g = 1$ and a lossless relative permittivity tensor $\varepsilon_g = [6.25, i0.06, 0; -i0.06, 6.25, 0; 0, 0, 6.25]$ under magnetization along z direction [33,34]. The standard structure of this study is shown in Fig. 1(a), which is composed of cylindrical BIG nanodisks with vertical side wall, whose diameter D and height H are 620 nm and 260 nm, respectively. The period of the nanodisk array P was set to be 850 nm. This structure is based on Ref. [17], in which ED and MD resonances under the EIT condition simultaneously enable the high T and large θ_f in the telecommunication wavelengths. To numerically analyze the structure, we employed the finite element method (FEM) for solving the Helmholtz equation under normal incidence of light using COMSOL Multiphysics. We constructed a triangular mesh first on the top surface of the unit cell and then over the entire structure using the swept function in COMSOL to make the generated mesh as uniform as possible. We assumed the incidence of plane wave propagating along z direction from $6 \mu\text{m}$ above the structure with fixed linear polarization parallel to x direction. The computational domain was filled with clad materials (in this case SiO_2) and was terminated by perfectly matched layers for z direction, while x and y boundaries were assumed to be periodic. Transmitted light was monitored $6 \mu\text{m}$ below the metasurface, from which we evaluated T and θ_f .

To investigate the influence of fabrication imperfections, we considered the tilt of the nanodisk side wall as the most-common deviation from the as-designed structure. With the tilt, the nanodisk takes the form of conical frustum as shown in Fig. 1(b). Each frustum is characterized

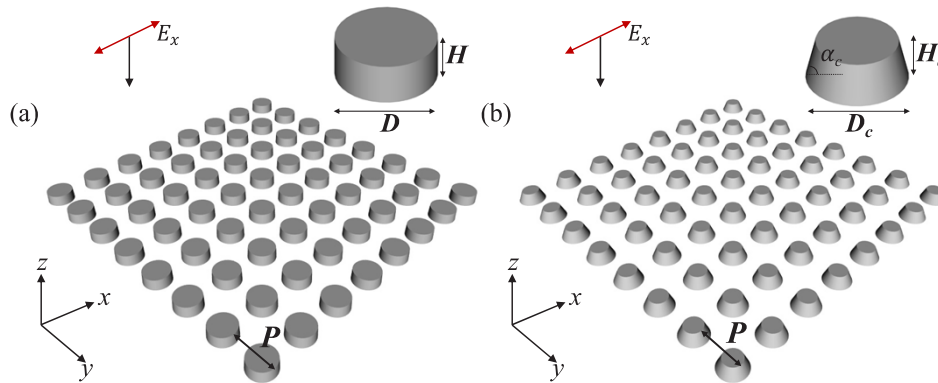


Fig. 1. (a) MO metasurface composed of a square array of BIG nanodisks with vertical side wall. The BIG nanodisks are embedded in SiO_2 . The right top inset shows the dimensions of single nanodisk. (b) MO metasurface with tilted side wall. Each nanodisk takes the form of a cone frustum characterized by a tilted sidewall angle of α_c as described in the right top inset.

by its base diameter D_c , height H_c and side wall angle of α_c . As we will demonstrate later, careful optimization of these parameters is important to attain large θ_f and T even when α_c is not vertical. Below, we will first discuss the standard structure with $\alpha_c = 90^\circ$ to understand the basics of the MO metasurface and then analyze the influence of the fabrication imperfections ($\alpha_c \neq 90^\circ$).

3. Results and discussions

3.1. As-designed BIG nanodisk array with vertical sidewall

First, we examined the standard structure with each BIG nanodisk having a vertical side wall. The P and D are set to be the standard value of 850 and 620 nm, respectively. Here, we treat height H as a variable to understand the behavior of the standard MO metasurface, which is governed by the ED and MD resonances shown in Fig. 2(a) and (b). To precisely identify the origins of these modes, multi-component decomposition is useful [35]. The two resonance modes are respectively doubly degenerated. When $H = 350$ nm, the two modes are spectrally detuned as shown in the transmission spectrum in Fig. 2(c). The ED and MD resonances are found at $\lambda_{ED} = 1381.5$ nm and $\lambda_{MD} = 1424.5$ nm, respectively. In this case, we do not see high T around the resonances. By changing H , the relative detuning between the ED and MD resonances can be controlled, as shown in the colormap plotted in Fig. 2(e). The diagonal sharp line across the plot is of the MD resonance. At $H = 258$ nm, the two modes recover the mutual resonance and a sharp transmittance peak of the MD mode due to EIT with T of near 100% was observed in the wide dip of the ED resonance as plotted in Fig. 2(d). The transmittance window is created by the constructive interference of the ED and MD modes in the transmission channel. Note that the spectral asymmetry of MD transmission peak ubiquitously observed in Fig. 2(e) arises from the Fano interference of the sharp MD mode with the broader ED resonance.

Interestingly, H does not only control the relative detuning between the ED and MD modes, but also Q factors and MO coupling strengths (κ) of them as shown in Fig. 2(f). Here, the Q factors were evaluated from the imaginary part of the eigenvalues of the computed optical modes. MO coupling strengths were evaluated from the eigenfrequency splittings of the computed two modes that are degenerated under zero magnetic field. The MO coupling strength can be naturally defined by the overlap integral of cross field product of the related two modes over the MO material under magnetic field [36]. For thicker H , the overlap integral tends to be larger so does κ . Meanwhile, the Q factor of the MD mode decreases with increasing H . In a perturbative theory

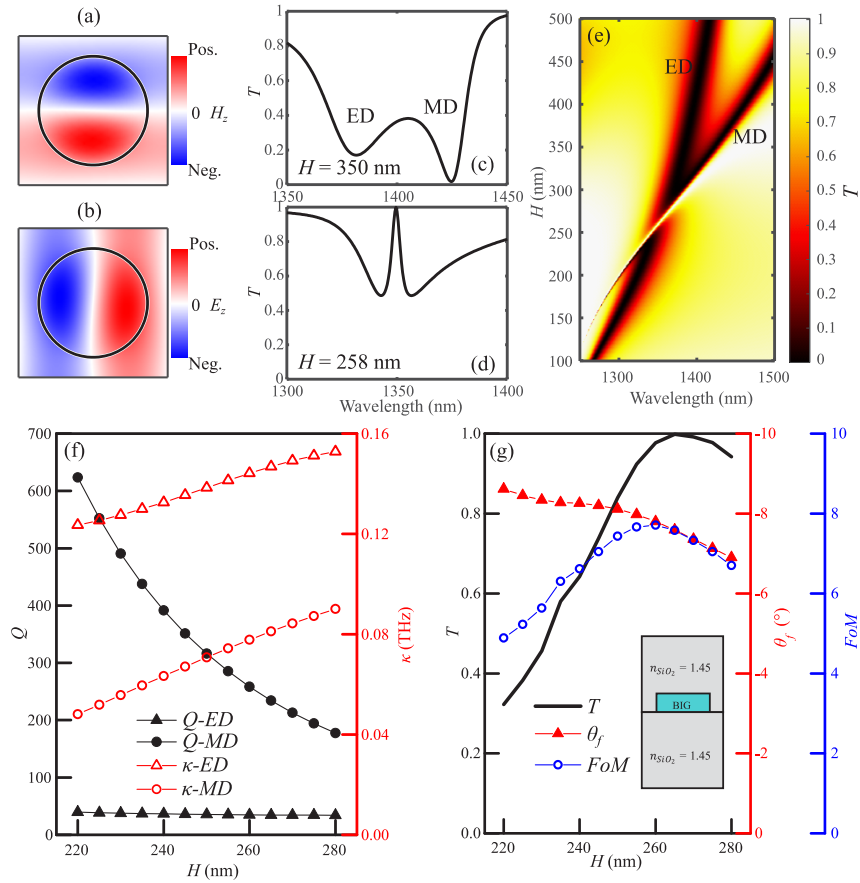


Fig. 2. Analysis of the MO metasurface with vertical sidewall. Field profiles of the (a) ED and (b) MD modes represented by z component of magnetic field (H_z) and electric field (E_z), respectively. Transmission spectra when (c) $H = 350$ nm and (d) $H = 258$ nm. (e) Colorplot of transmission spectra computed with varying H . The narrow diagonal line stems from the MD resonance. (f) H dependence of the Q factor and MO coupling strength κ of the ED and MD modes. (g) T , θ_f and FoM calculated as a function of H . At each parameter, T was evaluated at the wavelength where θ_f took the peak. The inset shows the cross section of a BIG nanodisk in the standard structure considered here.

[36], the product $\kappa \cdot Q$ is known to determine θ_f , which is dominated by the contribution from the MD modes in the current structure. Accordingly, the opposite behaviors of κ and Q when varying H make the change of $\kappa \cdot Q$ mild, and so do θ_f . This can be confirmed in Fig. 2(g), in which T , θ_f and FoM are plotted as a function of H . In this plot, T was evaluated at the wavelength where θ_f takes the peak value in each Faraday rotation spectrum. T varies largely since high transmittance is available only around the EIT condition as discussed above. Since θ_f is less dependent on H , FoM ($=\sqrt{T} \cdot |\theta_f|$) closely follows the behavior of T and takes the largest value of 7.6 around the EIT resonance ($H = 260$ nm).

3.2. Imperfect BIG nanodisk array with tilted sidewall

Now we examine the influence of fabrication imperfections by introducing inclination of the side wall ($\alpha_c < 90^\circ$) as illustrated in Fig. 3(a). Figure 3(b) shows the evolution of transmission

and Faraday rotation angle spectra when varying α_c . Note that, for nonvertical α_c , genuine ED and MD can no longer exist due to broken symmetry, and they will behave as ED-like and MD-like modes. The transmittance at the MD-like resonance peak shows a rapid reduction when decreasing α_c . The observed reduction of T arises from the degradation of optical interference between the light fields scattered by the ED-like and MD-like modes. Non-vertical α_c affects differently to the two types of modes and breaks their exact overlapping in the spectral domain. Moreover, the scattered field patterns by the ED-like and MD-like modes are altered differently by non-ideal α_c . This results in the degradation of the overlap between the two scattered fields in the spatial domain. The degradation of the interference both in the spectral and spatial domain strikingly diminishes the EIT effect and results in the rapid reduction of T . This tendency is summarized in Fig. 3(c). We observed 90% reduction of T when α_c reaches 78° .

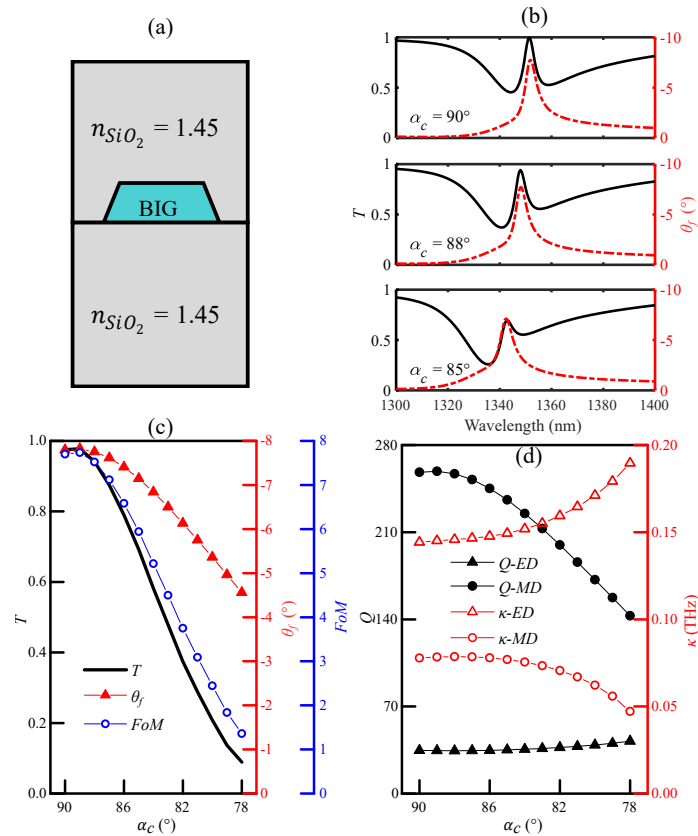


Fig. 3. Effect of sidewall angle α_c . (a) Illustration of BIG nanodisk with tilted sidewall embedded in SiO₂. (b) Evolution of transmission and Faraday rotation angle spectra with decreasing α_c . (c) Summary of T , θ_f and FoM as a function of α_c . (d) Q factor and κ of the ED-like and MD-like modes when varying α_c .

Meanwhile, we did not observe a significant reduction of θ_f measured at the MD resonance. This can be understood from Fig. 3(d), in which computed Q factors and κ are plotted as a function of α_c . We observed a 45% reduction of Q factor and 40% reduction of κ for the MD-like mode when decreasing α_c to 78° , which are much gentler compared with that of T . Interestingly, we observed the increases of Q and κ for the ED-like mode, which help in slightly increasing θ_f . Altogether, the degradation of θ_f was mild and hence the reduction of FoM is governed by the reduction of T , as seen in Fig. 3(b). This observation suggests that maintaining high T is the key

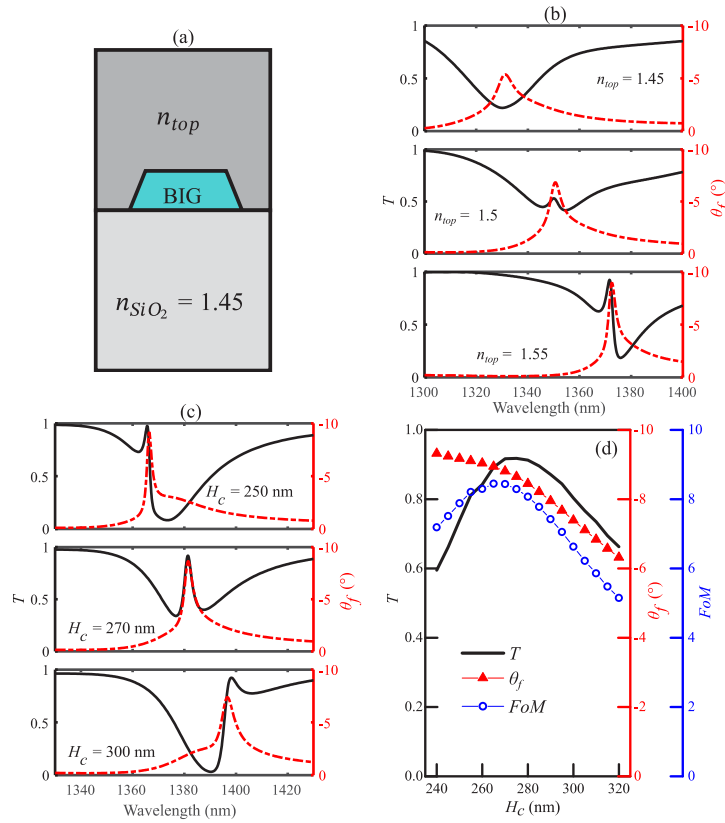


Fig. 4. (a) Illustration of an imperfect MO nanodisk cladded by a material with a different refractive index of n_{top} . (b) Transmission and Faraday rotation spectra of a MO metasurface of $\alpha_c = 80^\circ$ computed for different n_{top} ($P = 850$, $D = 620$, $H_c = 260$). (c) Transmission and Faraday rotation spectra of a MO metasurface of $\alpha_c = 80^\circ$ and $n_{top} = 1.55$ calculated for different height H_c ($P = 850$, $D = 620$). (d) T , θ_f and FoM as a function of H_c when $\alpha_c = 80^\circ$ and $n_{top} = 1.55$. T and FoM are collected at the wavelength of the largest θ_f at each H_c .

to attain high FoM even with nonideal α_c , akin to the case of the ideal structure with vertical side wall.

3.3. Changing the upper clad to recover FoM

So far, we have identified that a key to achieving a high FoM is to attain a high transmission, which is available only when high-quality EIT occurs in the device. However, with the tilted sidewall, it is unlikely to achieve a good spatial overlap of scattering fields from the ED-like and MD-like modes due to structural asymmetry in the vertical direction. We considered that the asymmetry could be mitigated by changing the refractive index of the upper clad (n_{top}) above the MO nanodisks as schematically shown in Fig. 4(a). The replacement of the upper cladding material can be straightforwardly adapted in most fabrication processes of optical metasurfaces.

Figure 4(b) shows the evolution of transmission and Faraday rotation spectra when varying n_{top} for the structure with tilted side wall of $\alpha_c = 80^\circ$ ($P = 860$ nm, $H_c = 260$ nm, $D_c = 620$ nm). For $n_{top} = 1.45$, which is the same with that of the bottom clad, we do not see any clear EIT peak in the broad dip of the ED-like mode. However, when increasing n_{top} above 1.5, we start to see a sharp EIT resonance of the MD-like mode in the dip. Moreover, the peak value of θ_f gradually

increases with increasing n_{top} . Figure 4(c) shows the changes of transmission and Faraday rotation spectra when varying H for the structure with $\alpha_c = 80^\circ$ and $n_{top} = 1.55$. Even in this case with the tilted side wall, akin to the case of the ideal structure discussed in Figs. 2(c)-(e), one can recover the EIT condition by tuning H . Surprisingly, when $H = 275$ nm, the transmittance reaches 92%, restoring a good EIT condition. Figure 4(d) summarizes T , θ_f and FoM as a function of H for the structure with $\alpha_c = 80^\circ$ and $n_{top} = 1.55$. The values of peak T and α_c are comparable with the ideal case in Fig. 2(f). Indeed, the maximum FoM is 8.4 ($\theta_f = 8.9^\circ$, $T = 89\%$ when $H_c = 265$ nm, which is even 9.5% increased than that of the ideal case. To observe such a high T in the actual experiment, the whole optical structure should be carefully designed to avoid unnecessary light reflection at various optical interfaces.

Finally, we inspect the versatility of our design for different side wall angle, α_c . We computed the optical responses of the structures with different α_c under different n_{top} of 1.45, 1.5, 1.55 and 1.6, as summarized in Fig. 5. The values of T and θ_f are of the structure exhibiting the maximum FoM that restored the EIT condition after optimizing H . For the symmetric cladding condition with $n_{top} = 1.45$, the highest performance is observed for the symmetric structure with $\alpha_c = 90^\circ$. Meanwhile, by increasing n_{top} , the best performance is observed at a nonvertical sidewall, $\alpha_c < 90^\circ$. This suggests that there is an optimal n_{top} for each α_c . In other words, one can recover the best performance for the structure with different α_c by tuning n_{top} . The maximally attainable FoM is comparable or even a bit larger than that of the ideal case. These results demonstrate that asymmetric cladding is a powerful way to achieve high performance in the MO metasurface with tilted sidewall. Meanwhile, to achieve significantly better performances compared to those

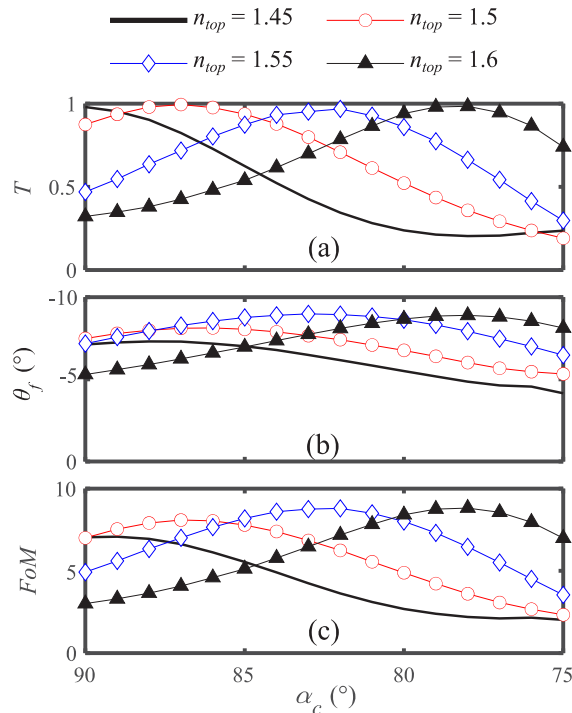


Fig. 5. T (top), θ_f (middle) and FoM (bottom) of MO metasurfaces of different n_{top} plotted as a function of α_c ($P = 850$ nm, $D = 620$ nm). Each data point was obtained when the EIT condition is restored by adjusting H_c . T and FoM were evaluated at the wavelength exhibiting the largest θ_f at each α_c .

realized in the current design, one may need to use totally different metasurface structures with much higher Q factors, such as those supporting dark modes [37,38].

Note that the observed recovery of high device performances could be associated with the result of interplay between the bianisotropy introduced by the tilted sidewalls and by the asymmetric top cladding. In this view, the asymmetric cladding could be interpreted to restore symmetry in the system by counteracting to the asymmetry introduced by tilting the sidewalls. Indeed, in a structure with an asymmetric cladding, we observed the disappearance of strong mode hybridization between the ED-like and MD-like modes, which usually occurs under the presence of bianisotropy (see Fig. 6 in Appendix).

4. Conclusions

We investigated the influence of tilted side walls for an all-dielectric MO metasurface operating at telecommunication wavelengths. We found that the non-verticality of the side wall rapidly degrades the FoM of the device, primarily due to the deterioration of T by diminishing the EIT effect. For a structure with an imperfect side wall angle of $\alpha_c = 78^\circ$, we observed a 91% reduction of T and an 82% smaller FoM , while Faraday rotation angle θ_f was only degraded by 42%. To recover the performance of the device, we introduced a top cladding material with a refractive index (n_{top}) different from that of the bottom (1.45). We showed that, even for a MO metasurface with $\alpha_c = 78^\circ$, near-unity T of 98% can be obtained by increasing n_{top} to 1.6 and recovering the EIT condition by tuning the height of the nanodisks. In this design, θ_f was -8.8° and the resulting FoM was 8.8, which is even 10% higher than that of the ideal case with vertical side wall. We also showed that such a high performance can be obtained for the structure with non-vertical α_c by optimizing n_{top} . The asymmetric cladding will be a powerful approach to realizing high performance all-dielectric MO metasurface even under the presence of imperfect sidewalls in the constituent elements.

Appendix

This appendix section discusses a possible mechanism for the observed recovery of the device performance by the asymmetric top cladding that we introduced in this work. Figure 6(a) plots a summary of computed eigenfrequencies of the ED-like and MD-like modes when $\alpha_c = 79^\circ$ and varying the height of the BIG resonators. In this case, the resonators are symmetrically cladded with the same material with the bottom cladding to inspect the influence of the bianisotropy introduced solely by the tilted sidewalls. We observed a linear crossing of the two optical modes akin to the case with vertical sidewalls. The linear crossing suggests that the mode hybridization between the ED-like and MD-like modes is weak compared to the optical losses in the examined structure. This observation ensures the presence of “independent” ED-like and MD-like modes in the system, being in line with our physical interpretations presented in the main text. The linear crossing was observed till $\alpha_c > 75^\circ$, covering the entire parameter range discussions in the main text. Meanwhile, when we further tilt the sidewall to $\alpha_c = 72^\circ$, we observed a clear anti-crossing of the two modes, as plotted in Fig. 6(b). This observation clearly demonstrates the formation of hybridized modes due to the strong coupling through the bianisotropy induced by the sidewall tilt. Interestingly, we can cancel out the observed strong coupling by introducing an asymmetric top cladding as shown in Fig. 6(c). We observed a linear crossing in this case, which indicates that the bianisotropy of the asymmetric cladding counteracts to that induced by the tilted sidewall. In this view, the asymmetric cladding could be interpreted to restore symmetry in the system. Careful comparisons with the behaviors of existing bianisotropic metasurfaces [39–41] and developing analytical models well-describing the observation will be essential to make the above interpretation more conclusive.

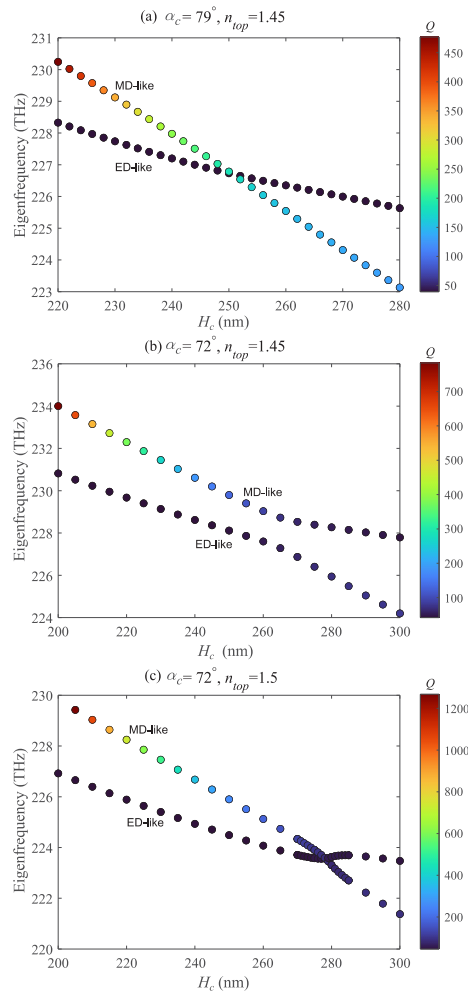


Fig. 6. Simulated eigenfrequencies of the ED-like and MD-like modes when the sidewall angle (a) $\alpha_C = 79^\circ$ with $n_{top} = 1.45$, (b) 70° with $n_{top} = 1.45$ and (c) 72° with $n_{top} = 1.5$.

Funding. Japan Society for the Promotion of Science KAKENHI (17H06138, 19K05300, 22H00298, 22H01994, 22K18989); Japan Science and Technology Agency CREST (JPMJCR19T1); Japan Science and Technology Agency FOREST Program (JPMJFR213F); Nippon Sheet Glass Foundation.

Acknowledgments. This work was supported by KAKENHI (17H06138, 19K05300, 22H00298, 22H01994, 22K18989), JST CREST (JPMJCR19T1), JST FOREST Program (JPMJFR213F), Nippon Sheet Glass Foundation.

Disclosures. The authors declare no conflicts of interest.

Data availability. Data underlying the results presented in this paper are available in Refs. [33,34].

References

1. M. C. Onbasli, L. Beran, M. Zahradník, M. Kučera, R. Antoš, J. Mistrík, G. F. Dionne, M. Veis, and C. A. Ross, "Optical and magneto-optical behavior of Cerium Yttrium Iron Garnet thin films at wavelengths of 200–1770nm," *Sci. Rep.* **6**(1), 23640 (2016).
2. M. Inoue, K. Arai, T. Fujii, and M. Abe, "One-dimensional magnetophotonic crystals," *J. Appl. Phys.* **85**(8), 5768–5770 (1999).
3. A. B. Khanikaev, A. B. Baryshev, P. B. Lim, H. Uchida, M. Inoue, A. G. Zhdanov, A. A. Fedyanin, A. I. Maydykovskiy, and O. A. Aktsipetrov, "Nonlinear Verdet law in magnetophotonic crystals: Interrelation between Faraday and Borrmann effects," *Phys. Rev. B* **78**(19), 193102 (2008).

4. M. A. Kozhaev, A. I. Chernov, D. A. Sylgacheva, A. N. Shaposhnikov, A. R. Prokopov, V. N. Berzhansky, A. K. Zvezdin, and V. I. Belotelov, "Giant peak of the Inverse Faraday effect in the band gap of magnetophotonic microcavity," *Sci. Rep.* **8**(1), 11435 (2018).
5. M. J. Steel, M. Levy, and R. M. Osgood, "High transmission enhanced Faraday rotation in one-dimensional photonic crystals with defects," *IEEE Photonics Technol. Lett.* **12**(9), 1171–1173 (2000).
6. H. Kato, T. Matsushita, A. Takayama, M. Egawa, K. Nishimura, and M. Inoue, "Effect of optical losses on optical and magneto-optical properties of one-dimensional magnetophotonic crystals for use in optical isolator devices," *Opt. Commun.* **219**(1-6), 271–276 (2003).
7. S. Kharratian, H. Urey, and M. C. Onbaşlı, "Broadband Enhancement of Faraday Effect Using Magnetoplasmonic Metasurfaces," *Plasmonics* **16**(2), 521–531 (2021).
8. V. I. Belotelov, L. L. Doskolovich, V. A. Kotov, E. A. Bezus, D. A. Bykov, and A. K. Zvezdin, "Magneto-optical effects in the metal-dielectric gratings," *Opt. Commun.* **278**(1), 104–109 (2007).
9. A. V. Baryshev, H. Uchida, and M. Inoue, "Peculiarities of plasmon-modified magneto-optical response of gold-garnet structures," *J. Opt. Soc. Am. B* **30**(9), 2371 (2013).
10. E. Almpanis, P.-A. Pantazopoulos, N. Papanikolaou, V. Yannopoulos, and N. Stefanou, "Metal-nanoparticle arrays on a magnetic garnet film for tunable plasmon-enhanced Faraday rotation," *J. Opt. Soc. Am. B* **33**(12), 2609 (2016).
11. A. B. Khanikaev, A. V. Baryshev, A. A. Fedyanin, A. B. Granovsky, and M. Inoue, "Anomalous Faraday effect of a system with extraordinary optical transmittance," *Opt. Express* **15**(11), 6612 (2007).
12. A. B. Khanikaev, S. H. Mousavi, G. Shvets, and Y. S. Kivshar, "One-Way Extraordinary Optical Transmission and Nonreciprocal Spoof Plasmons," *Phys. Rev. Lett.* **105**(12), 126804 (2010).
13. A. V. Baryshev and A. M. Merzlikin, "Tunable plasmonic thin magneto-optical wave plate," *J. Opt. Soc. Am. B* **33**(7), 1399 (2016).
14. D. Floess, J. Y. Chin, A. Kawatani, D. Dregely, H.-U. Habermeier, T. Weiss, and H. Giessen, "Tunable and switchable polarization rotation with non-reciprocal plasmonic thin films at designated wavelengths," *Light: Sci. Appl.* **4**(5), e284 (2015).
15. D. Li, L. Chen, C. Lei, J. L. Menendez, C. Mallada, Z. Tang, S. Tang, and Y. Du, "Plasmon-enhanced magneto-optical activity in a nanostructure with circle annular arrays," *J. Opt. Soc. Am. B* **33**(5), 922 (2016).
16. S. H. Mousavi, A. B. Khanikaev, J. Allen, M. Allen, and G. Shvets, "Gyromagnetically Induced Transparency of Metasurfaces," *Phys. Rev. Lett.* **112**(11), 117402 (2014).
17. A. Christofi, Y. Kawaguchi, A. Alù, and A. B. Khanikaev, "Giant enhancement of Faraday rotation due to electromagnetically induced transparency in all-dielectric magneto-optical metasurfaces," *Opt. Lett.* **43**(8), 1838 (2018).
18. A. I. Kuznetsov, A. E. Miroshnichenko, M. L. Brongersma, Y. S. Kivshar, and B. Luk'yanchuk, "Optically resonant dielectric nanostructures," *Science* **354**(6314), aag2472 (2016).
19. J. M. Geffrin, B. García-Cámara, R. Gómez-Medina, P. Albella, L. S. Froufe-Pérez, C. Eyraud, A. Litman, R. Vaillon, F. González, M. Nieto-Vesperinas, J. J. Sáenz, and F. Moreno, "Magnetic and electric coherence in forward- and back-scattered electromagnetic waves by a single dielectric subwavelength sphere," *Nat. Commun.* **3**(1), 1171 (2012).
20. M. Decker, I. Staude, M. Falkner, J. Domínguez, D. N. Neshev, I. Brener, T. Pertsch, and Y. S. Kivshar, "High-Efficiency Dielectric Huygens' Surfaces," *Adv. Opt. Mater.* **3**(6), 813–820 (2015).
21. A. Epstein and G. V. Eleftheriades, "Huygens' metasurfaces via the equivalence principle: design and applications," *J. Opt. Soc. Am. B* **33**(2), A31 (2016).
22. T. Kiel, P. Varytis, B. Beverungen, P. T. Kristensen, and K. Busch, "Enhanced Faraday rotation by dielectric metasurfaces with Bayesian shape-optimized scatterers," *Opt. Lett.* **46**(7), 1720 (2021).
23. D. O. Ignatyeva, D. M. Krichevsky, V. I. Belotelov, F. Royer, S. Dash, and M. Levy, "All-dielectric magneto-photonics metasurfaces," *J. Appl. Phys.* **132**(10), 100902 (2022).
24. L. Magdenko, E. Popova, M. Vanwolleghem, C. Pang, F. Fortuna, T. Maroutian, P. Beauvillain, N. Keller, and B. Dagens, "Wafer-scale fabrication of magneto-photonics structures in Bismuth Iron Garnet thin film," *Microelectron. Eng.* **87**(11), 2437–2442 (2010).
25. P. Pirro, T. Brächer, A. V. Chumak, B. Lägél, C. Dubs, O. Surzhenko, P. Görnert, B. Leven, and B. Hillebrands, "Spin-wave excitation and propagation in microstructured waveguides of yttrium iron garnet/Pt bilayers," *Appl. Phys. Lett.* **104**(1), 012402 (2014).
26. S. Li, W. Zhang, J. Ding, J. E. Pearson, V. Novosad, and A. Hoffmann, "Epitaxial patterning of nanometer-thick $Y_3Fe_5O_{12}$ films with low magnetic damping," *Nanoscale* **8**(1), 388–394 (2016).
27. N. Zhu, H. Chang, A. Franson, T. Liu, X. Zhang, E. Johnston-Halperin, M. Wu, and H. X. Tang, "Patterned growth of crystalline $Y_3Fe_5O_{12}$ nanostructures with engineered magnetic shape anisotropy," *Appl. Phys. Lett.* **110**(25), 4–9 (2017).
28. N. Sugimoto, Y. Katoh, A. Tate, and A. Shibukawa, "Preparation of Substituted $Y_3Fe_5O_{12}$ Waveguide Directional Coupler Using Ion-Beam Etching," *Jpn. J. Appl. Phys.* **32**(Part 2, No. 1A), L65–L67 (1993).
29. D. O. Ignatyeva, D. Karki, A. A. Voronov, M. A. Kozhaev, D. M. Krichevsky, A. I. Chernov, M. Levy, and V. I. Belotelov, "All-dielectric magnetic metasurface for advanced light control in dual polarizations combined with high-Q resonances," *Nat. Commun.* **11**(1), 5487 (2020).
30. A. A. Voronov, D. Karki, D. O. Ignatyeva, M. A. Kozhaev, M. Levy, and V. I. Belotelov, "Magneto-optics of subwavelength all-dielectric gratings," *Opt. Express* **28**(12), 17988 (2020).

31. M. G. Barsukova, A. S. Shorokhov, A. I. Musorin, D. N. Neshev, Y. S. Kivshar, and A. A. Fedyanin, "Magneto-Optical Response Enhanced by Mie Resonances in Nanoantennas," *ACS Photonics* **4**(10), 2390–2395 (2017).
32. S. Xia, D. O. Ignatyeva, Q. Liu, J. Qin, T. Kang, W. Yang, Y. Chen, H. Duan, L. Deng, D. Long, M. Veis, V. I. Belotelov, and L. Bi, "Enhancement of the Faraday Effect and Magneto-optical Figure of Merit in All-Dielectric Metasurfaces," *ACS Photonics* **9**(4), 1240–1247 (2022).
33. T. Tepper and C. A. Ross, "Pulsed laser deposition and refractive index measurement of fully substituted bismuth iron garnet films," *J. Cryst. Growth* **255**(3-4), 324–331 (2003).
34. Z. Yu, Z. Wang, and S. Fan, "One-way total reflection with one-dimensional magneto-optical photonic crystals," *Appl. Phys. Lett.* **90**(12), 1–4 (2007).
35. A. B. Evlyukhin and B. N. Chichkov, "Multipole decompositions for directional light scattering," *Phys. Rev. B* **100**(12), 125415 (2019).
36. Z. Wang and S. Fan, "Magneto-optical defects in two-dimensional photonic crystals," *Appl. Phys. B* **81**(2-3), 369–375 (2005).
37. Y. Yang, I. I. Kravchenko, D. P. Briggs, and J. Valentine, "All-dielectric metasurface analogue of electromagnetically induced transparency," *Nat. Commun.* **5**(1), 5753 (2014).
38. D. R. Abujetas, Á. Barreda, F. Moreno, A. Litman, J. Geffrin, and J. A. Sánchez-Gil, "High-Q Transparency Band in All-Dielectric Metasurfaces Induced by a Quasi Bound State in the Continuum," *Laser Photonics Rev.* **15**(1), 2000263 (2021).
39. A. E. Miroschnichenko, A. B. Evlyukhin, Y. S. Kivshar, and B. N. Chichkov, "Substrate-Induced Resonant Magneto-electric Effects for Dielectric Nanoparticles," *ACS Photonics* **2**(10), 1423–1428 (2015).
40. M. Odit, P. Kapitanova, P. Belov, R. Alaei, C. Rockstuhl, and Y. S. Kivshar, "Experimental realisation of all-dielectric bianisotropic metasurfaces," *Appl. Phys. Lett.* **108**(22), 221903 (2016).
41. A. Slobozhanyuk, A. V. Shchelokova, X. Ni, S. Hossein Mousavi, D. A. Smirnova, P. A. Belov, A. Alù, Y. S. Kivshar, and A. B. Khanikaev, "Near-field imaging of spin-locked edge states in all-dielectric topological metasurfaces," *Appl. Phys. Lett.* **114**(3), 031103 (2019).